Remote Sens. **2011**, *3*, 2420-2439; doi:10.3390/rs3112420

OPEN ACCESS

Remote Sensing

ISSN 2072-4292

www.mdpi.com/journal/remotesensing

Article

Object-Based Image Analysis of Downed Logs in Disturbed Forested Landscapes Using Lidar

Samuel D. Blanchard, Marek K. Jakubowski and Maggi Kelly *

Department of Environmental Sciences, Policy, and Management, College of Natural Resources, University of California at Berkeley, Berkeley, CA 94720, USA;
E-Mails: sablanchard@berkeley.edu (S.D.B.); marek@berkeley.edu (M.K.J.)

* Author to whom correspondence should be addressed; E-Mail: maggi@berkeley.edu.

Received: 20 September 2011; in revised form: 9 November 2011 / Accepted: 10 November 2011 / Published: 16 November 2011

Abstract: Downed logs on the forest floor provide habitat for species, fuel for forest fires, and function as a key component of forest nutrient cycling and carbon storage. Ground-based field surveying is a conventional method for mapping and characterizing downed logs but is limited. In addition, optical remote sensing methods have not been able to map these ground targets due to the lack of optical sensor penetrability into the forest canopy and limited sensor spectral and spatial resolutions. Lidar (light detection and ranging) sensors have become a more viable and common data source in forest science for detailed mapping of forest structure. This study evaluates the utility of discrete, multiple return airborne lidar-derived data for image object segmentation and classification of downed logs in a disturbed forested landscape and the efficiency of rule-based object-based image analysis (OBIA) and classification algorithms. Downed log objects were successfully delineated and classified from lidar derived metrics using an OBIA framework. 73% of digitized downed logs were completely or partially classified correctly. Over classification occurred in areas with large numbers of logs clustered in close proximity to one another and in areas with vegetation and tree canopy. The OBIA methods were found to be effective but inefficient in terms of automation and analyst's time in the delineation and classification of downed logs in the lidar data.

Keywords: lidar; Object-Based Image Analysis (OBIA); downed logs; downed dead wood

1. Introduction

Dead woody material on the forest floor is an essential structural component of forest ecosystems: downed dead wood provides habitat for species, is a fuel source for forest fires, and is a key component of forest nutrient cycling and carbon storage [1-3]. Information on the quantity and location of downed logs in forests is important for assessing fire risk [4,5], measuring dead biomass for carbon storage estimates [6], biodiversity and nutrient cycling [7,8], forest management and silviculture [9,10], and wildlife habitat monitoring and modeling [11].

Methods for mapping and characterizing downed logs in forests have traditionally relied on ground-based field surveys with and without Global Positioning Systems (GPS) technology [8,12]. Field surveys remain relevant data collection methods, but they are increasingly being supplemented by satellite-based and aerial-based remotely sensed data [13]. Ground-based field methods are limited in their spatial extent due to practical constraints on time, cost, resources, and site accessibility. Downed logs are usually distributed in a non-uniform pattern and are not spatially contiguous on the forest floor; extensive and complex field campaigns are sometimes necessary to locate and characterize logs. In addition the unit of analysis in ground-based surveys is usually limited to the size of individual survey plots which can lead to under- and over-generalization of the landscape [13].

The objective of this study is to examine the efficacy of object-based image analysis methods for identifying and quantifying downed logs in disturbed forested landscapes using airborne lidar data. This study evaluates the utility of airborne lidar derived data products for image object segmentation and classification of downed logs and the efficiency of rule-based OBIA and classification algorithms. This research was motivated by the desire to investigate how well these important forest structural features could be automatically extracted from the lidar data. If successful, this would be a benefit to researchers who are studying forest fuels for fire modeling, and for wildlife experts studying how species utilize the forest.

1.1. Remote Sensing and Lidar in Forest Science

The fields of forest ecology and forest management have embraced remote sensing approaches for many routine and innovative applications. Moderate spatial resolution (5–30 m) imagery from Landsat, Advanced Spaceborne Thermal Emission and Reflection Radiometer (ASTER), and Système Pour l'Observation de la Terre (SPOT) sensors have been used to map forest pattern and large-scale disturbance [14,15]. Fine spatial resolution imagery (<5 m) from digital aerial orthophotographs, IKONOS, QuickBird, and Worldview-2 sensors are commonly used to map vegetation abundance and productivity [16,17], monitor disturbances and change [18-21], and assist in forest management [22]. These passive image sources offer advantages over traditional field based approaches in their repeatability, lower acquisition cost, and greater spatial extent, but they are limited by their top-of-canopy perspective which reduces the ability to observe objects below the canopy [17,23-25]. These data are also constrained in the size of objects that can be observed with their spatial and spectral resolutions.

Within the past 10 years other remotely sensed data sources such as airborne light detection and ranging (lidar) have become a more viable and common data source in forest science for detailed

mapping of forest structure [23,24]. The lidar instrument emits and captures laser pulses, allowing for calculation of the 3-dimensional position of a reflecting target [23,24,26-28]. Lidar data can be captured from aircraft-mounted instruments (airborne lidar) or from ground-based systems (ground-based lidar). Airborne lidar systems are classified based on whether they record the range to the first or last return (single return), multiple returns, or fully digitize the return signal (full waveform lidar), and whether they have a small (typically about a meter) or large (tens of meters) laser illumination area or footprint [26]. In most cases, lidar data is delivered as a point cloud—a collection of points with x, y, z positions and their recorded light intensities. In a forest, these returns can be reflected from the ground, leaves, branches, and trunks of trees. The point cloud can be classified into ground returns, which are commonly interpolated to a fine spatial resolution digital terrain model (DTM), and above-ground returns, which are used to map forest structure. Often the above-ground points are interpolated to a canopy height model: a raster surface of forest heights.

While the use of lidar is limited by its relatively high acquisition cost, small spatial extent, and data processing complexity [29], lidar offers several advantages over passive sensors. Lidar data are flexible, in scale and format: lidar data can be analyzed as a collection of points, as a derived raster layer, or as a series of raster layers. The ability of the lidar pulse to penetrate the forest canopy to the forest floor allows for fine spatial resolution mapping of canopy and understory vegetation across vertical and horizontal domains, and allows for the mapping of ground topography and structure [23,24,30].

Lidar data has been used for a variety of applications in forest science at a variety of scales. At the stand scale, lidar can be used to map general forest characteristics [31], as well as more detailed measurements such as stem volume [32], biomass [33,34], and leaf area index (LAI) [35]. At finer scales, a number of studies have focused on extracting individual trees from the lidar cloud or from the canopy height model [36-41], or from the intensity data associated with the lidar returns [42]. In addition to the topographic information required in fire behavioral models [30], the structural components of forests, such as canopy height, canopy cover, crown base height (CBH), crown bulk density (CBD), total basal area, shrub height, and shrub cover have been mapped successfully with lidar data [43-46]. Individual components of forest fuels—surface litter and downed wood—have not yet been successfully mapped using lidar.

Additionally, lidar data have been used to map the structural elements in a forest that are important for wildlife habitat [24,47-50]. Goetz *et al.* [51] used airborne lidar data to calculate an index of vertical structure to use in habitat models predicting avian species richness. Seavy *et al.* [25] used small footprint lidar to describe habitat associations of riparian passerine birds. Müller *et al.* [52] found that structural factors in lidar data (mean canopy height, the standard deviation of mean canopy height, and the maximum height of canopy calculated from the digital crown model) better predicted bird assemblages than field data alone in Germany.

Despite these many approaches to mapping forests with lidar, there are few examples of studies utilizing lidar to map downed logs on the forest floor. The majority of studies assessing and mapping dead wood with lidar have done so by characterizing and mapping dead standing trees (also called snags) (e.g., [53]). Lidar has also been used to estimate coarse woody debris volumes in non-disturbed forested landscapes (e.g., [7]) but lidar has not widely been used to map individual discrete downed log objects in a disturbed forested landscape.

1.2. Object-Based Image Analysis and Forest Science

In both optical remote sensing and in lidar data there is a trend towards increasing detail in mapping. The importance in forest science of the ability to extract individual objects in the forest is increasingly noted. Precise mapping of individual trees or shrubs in a forest aids in understanding forest biometeorology [37], tree demography [20], community structure [54], carbon storage [23,55], pathogen spread [56,57], and habitat use [47,53]. The need for object-based precision in mapping can in some cases be facilitated by a field of image segmentation and classification procedures commonly called object-based image analysis (OBIA).

OBIA is an image processing and analysis framework in which image classification and subsequent analysis focuses on discrete groups of similar pixels, rather than on individual pixels [58,59]. OBIA segmentation can create image objects that closely resemble the size and shape of features in the real world scene as represented in the data [60]. An OBIA approach allows for the use of multiple dimensions and scales of data and spatial metrics such as neighborhood, topology, and feature statistics in image classification, as opposed to pixel-based methods, which rely on the single dimension of a pixel's digital value. Image objects can operate at the spatial scale of the real world features represented in the data and image objects can allow for the incorporation of expert knowledge into the creation and classification of objects [60,61].

There are several benefits of OBIA over pixel-based classification methods. Most commonly cited are the higher classification accuracies and computational efficiencies of OBIA compared with pixel-based classification algorithms, especially with fine-scale imagery [62,63]. Image objects also capture useful features (e.g., shape, texture, and context relations with other objects) that single pixels lack, and can be organized hierarchically, capturing multi-scalar relationships between objects [59,64-66]. The segmentation and classification process can be cumbersome and complicated, however, with multiple results possible [66].

In forest science, OBIA approaches have been used with fine-scale imagery for forest type mapping and stand delineation [60,67-71], and to track disturbances and forest change [19,21,72]. Many of these examples use optical imagery alone, without lidar. Some exceptions exist. For example, Antonarakis *et al.* [31] used elevation and lidar intensity data to broadly classify forest and ground types using a supervised object orientated approach. The OBIA approach was used primarily as a broad discriminator so that multispectral classification could be used in the resulting areas. Arroyo *et al.* [73] integrated discrete return (4 returns) lidar data with QuickBird imagery in an OBIA framework to estimate riparian forest parameters in Queensland, Australia. This work was also discussed in Johansen *et al.* [74]. Sullivan *et al.* [70] created stand maps for forests near Olympia, Washington using discrete return (4 returns) lidar data in an OBIA framework. Pascual *et al.* [75] used an object-based approach with the canopy height model from small footprint, discrete (2 returns) lidar data to characterize the structure of *Pinus sylvestris* L. stands in forests of central Spain. Johansen *et al.* [76] used an OBIA approach with discrete (2 returns) lidar data to map riparian zones. These applications are summarized in Table 1. None used an OBIA approach to isolate small forest features such as downed logs.

Table 1. Summary of select literature in forest science utilizing object-based image analysis*.

Remotely Sensed Input Data	Location	Application	Reference
Landsat ETM+	British Columbia, Canada	Land cover & logging scar classification	[61]
DAIS	Point Reyes, California. USA	Vegetation species classification	[71]
IKONOS	Flanders, Belgium	Forest land cover classification	[67]
IKONOS	Marin County, California, USA	Forest edge mapping	[72]
IKONOS	Western Alberta, Canada	Forest inventory mapping	[60]
IKONOS	British Columbia, Canada	Forest inventory mapping	[68]
IKONOS	North Carolina, USA	Forest type mapping	[42]
ADAR	China Camp State Park, California, USA	Tree mortality classification	[19,21]
QuickBird	Madrid, Spain	Fire fuel type mapping	[77]
QuickBird + Lidar (discrete, 4 return)	Central Queensland, Australia	Riparian biodiversity and wildlife habitats	[73,74]
CIR digital aerial photography (0.5m)	Great Smoky Mountains National Park, USA	Forest type mapping	[78]
Lidar (discrete, 4 returns)	Olympia, Washington, USA	Forest stand mapping	[70]
Lidar (discrete, 2 returns)	Central Spain	Forest inventory mapping	[75]
Lidar (discrete, 2 returns)	Victoria, Australia	Riparian forest mapping	[76]
SPOT + Lidar (discrete, 2 returns)	Garonne & Allier rivers, France	Land cover & forest age classification	[31]

*Note: Lidar: light detection and ranging; ETM: Enhanced Thematic Mapper; DAIS: Digital Airborne Imaging System; ADAR: Airborne Data Acquisition and Registration; CIR: Color Infrared; SPOT: Système Pour l'Observation de la Terre.

2. Study Area

The study area (centered at 120°30′30″W, 39°8′20″N) is located near Last Chance in Placer County, California, USA (Figure 1). The study area is an 11 ha subset of a larger study area located within the Tahoe National Forest. This study is part of a larger project, the Sierra Nevada Adaptive Management Project (SNAMP), a multidisciplinary study on the ecological and social effects of forest fuels treatments [79]. Elevation in the subset study area ranges from 1,918 to 2,085 m with a mean height of 1,977 m. The subset study area has a mean slope of 20 and a standard deviation of 7°. Land cover in the subset study area is dominated by bare ground and low lying shrubs with a maximum height of approximately 30 cm, and has an isolated pocket of conifer trees that range from 10 to 60 m in height.

Through extensive fieldwork, the subset study area was identified as an optimal candidate to evaluate the detection and classification of downed logs using object based image analysis methods because of the site's low canopy cover and lack of dense vegetation. The site was burned by the Star Forest Fire in 2001, eight years prior to the acquisition of the lidar data. The fire disturbance and lack of dense canopy cover facilitates a concentrated and large sample of downed logs, enables visual verification of downed logs from remotely sensed data, and allows for greater lidar ground point vertical accuracies with the absence of canopy cover.

Figure 1. Study area in Northern California, USA: **(a)** the Last Chance study area in the Tahoe National Forest; **(b)** NAIP image of the subset study area used in this work; and **(c)** a ground photograph of the study area looking southeast.

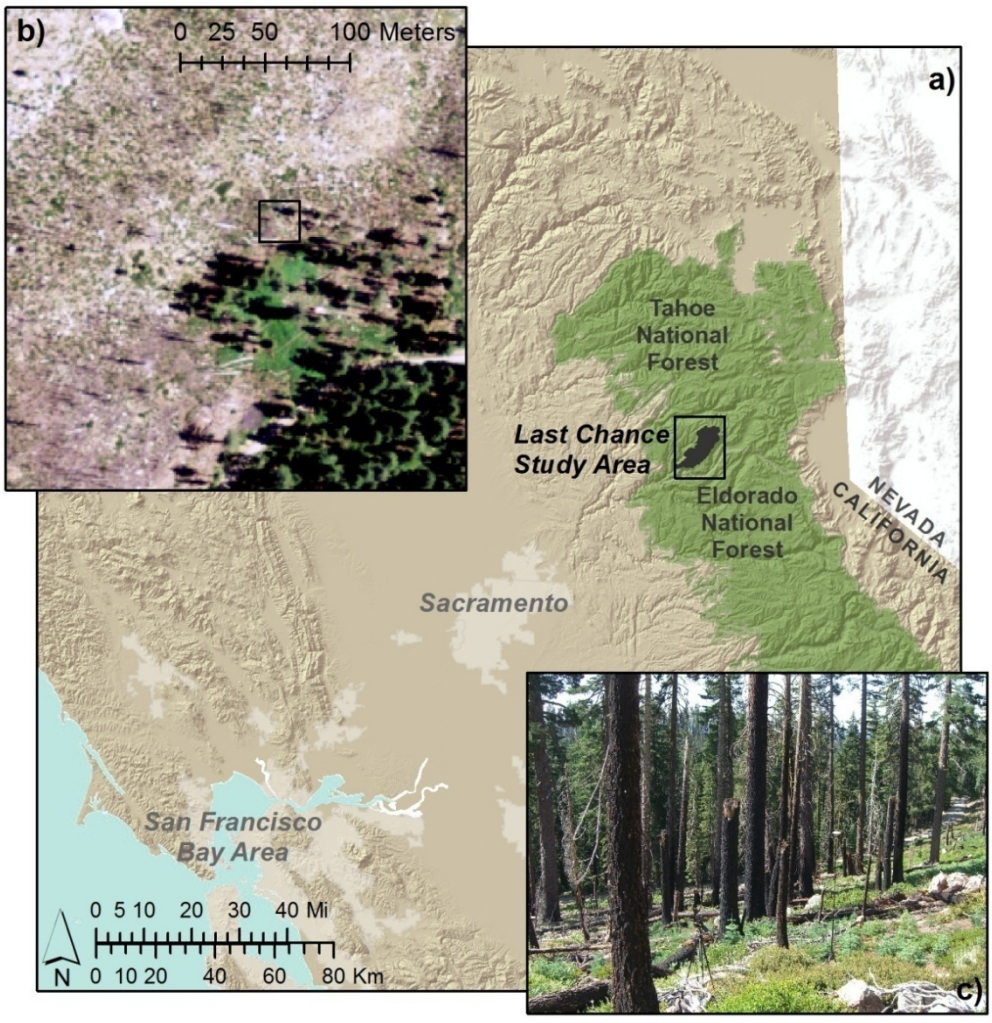

3. Data

3.1. Lidar Data

Lidar data was acquired from five survey flights from 18 to 22 September 2008. Lidar data was flown and processed by the National Center for Airborne Laser Mapping (NCALM), a collaboration between the University of Houston and the University of California, Berkeley [80]. An Optech GEMINI Airborne Laser Terrain Mapper (ALTM) with a horizontal accuracy of 5–10 cm and vertical

accuracy of 5 cm, was flown at an approximate altitude of 1,000 m above ground level [30]. The sensor captured four returns per pulse. Data was collected for a total area of 107 km^2 at an average density of at least 9 pulses per m^2. The point density often exceeded 20 returns per square meter in dense forest canopy. An 11 ha subset of the lidar data was selected for the study area which has a density of 10.5 points per square meter. The survey had an average swath width of 581 m for a single pass and used a 70 KHz pulse rate frequency. Steep terrain throughout the survey area and the desire to utilize the more reliable single-pulse mode limited the pulse rate frequency to 70 KHz [30].

The survey's absolute calibration used 1,274 check points from three GPS reference stations with horizontal and vertical accuracies of 1.2 cm. The final lidar data product had a swath height disagreement of 7.5 cm and an overall horizontal accuracy of 5–10 cm and vertical accuracy of 5 cm. Intensities have been normalized using the standard square of the range algorithm [30]. Lidar data processing and classification was completed in Terrasolid's TerraScan software [81]. The last return lidar points were classified into four categories: above ground, ground, building, and low points. The bare-earth model was created from ground points only. The ground points were classified using an iteratively building Triangulated Irregular Network (TIN) surface algorithm and outlier points below the resulting surface were filtered and removed. More information on the technical specifications for the ALTM sensor, survey, and lidar data can be found in Guo *et al.* [30].

Figure 2. Digitized downed logs validation data.

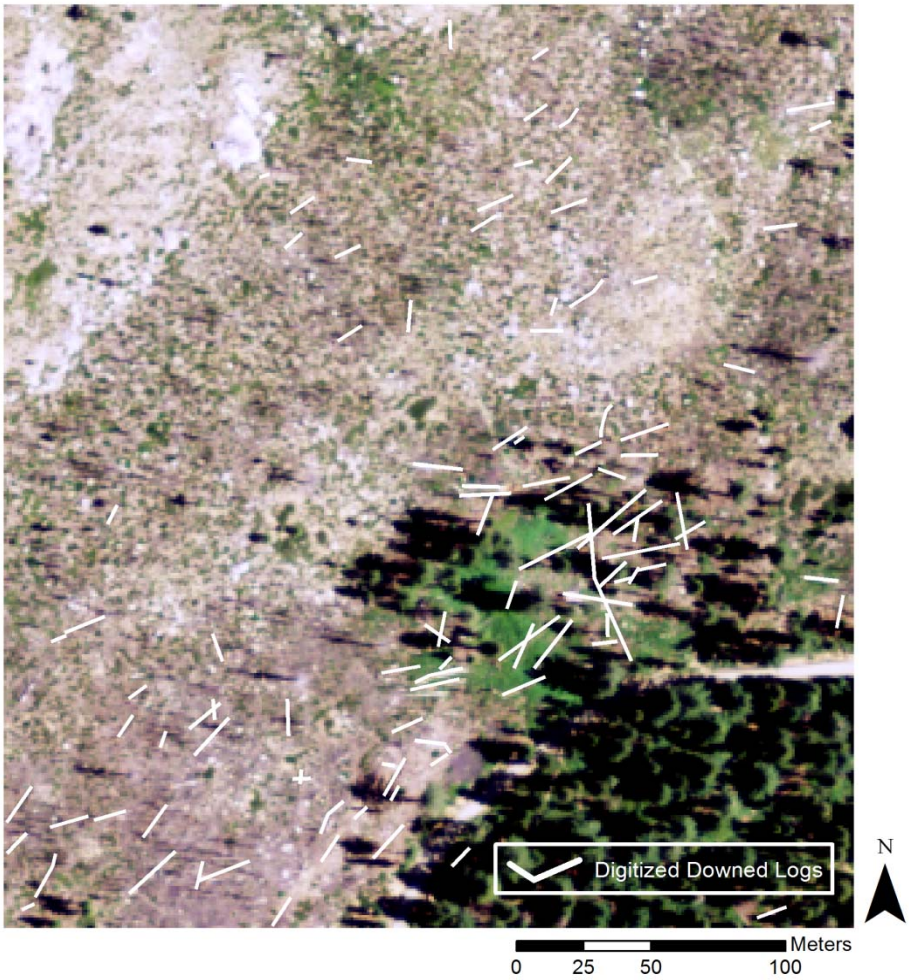

3.2. Downed Log Validation Data

A total of 103 individual downed log segments were identified to validate the OBIA results (Figure 2). The downed logs were visually identified using the lidar ground point data in combination with the National Agriculture Imagery Program (NAIP) color orthophotographs acquired over the study area in July 2009. The NAIP orthophotographs have a 1 m spatial resolution and a 6 m horizontal accuracy [82]. The target logs are clearly visible and identifiable in the lidar data; these data, along with ground photographs were used to manually digitize downed logs (Figure 2).

4. Methods

4.1. Object-Based Image Analysis Input Layers

The processed last return lidar points classified as ground were rasterized at a spatial resolution of 0.5 m. This spatial resolution allows for optimal object size and data retention from point to grid cell. The downed logs in this study area are well represented at 0.5 m spatial resolution because their width ranges from 25 cm to 1.5 m and length ranges from 5 to 30 m. Further, the typical horizontal distance among lidar returns was small, such that at 0.5 m pixel size, each pixel contained an average of 2.2 points. Rasterizing the point cloud at a pixel size smaller than 0.5 m resulted in undesirable artifacts. Specifically, the collection pattern of the lidar sensor became apparent, which hinders further processing of the data. The point to raster conversion process assigns raster cell values based on a specified metric or statistic, such as the mean or standard deviation, for all vector points that fall within a cell's boundaries. For example, to derive a raster image of mean elevation, the mean value of all points within a cell will be calculated and entered as the cell's value.

The metrics listed in Table 2 were extracted and rasterized directly from the vector lidar point data. Metrics characterizing elevation and scene information were rasterized and include: elevation (standard deviation and minimum), total number of points, absolute roughness, intensity, point density, and slope. The metrics were selected based on the level of homogeneity in the pixel values and whether or not discrete and linear outlines of downed logs were readily discernible. The rasterized data was visually assessed for appropriate thresholds to highlight and enhance the separation between pixels and groups of pixels and also to enhance homogenous pixel clustering. A combination of filters and Boolean reclassifications were used to achieve the aforementioned characteristics. This was done to isolate the linear shapes of downed logs and to create data layers that optimize the distinction between log objects and non-log objects during image segmentation and object classification. A 3 × 3 high pass filter was applied to the elevation standard deviation layer and a 3 × 3 low pass, median, and Sobel filter were applied to the total number of points layer. Values in the filtered elevation standard deviation and the elevation minimum were reclassified. The input data is ranked in Table 2 from 1 to 11 in descending order from data that have the most homogenous pixel clusters and sharpest cluster boundary separation to those that have more heterogeneous pixel clusters and ambiguous cluster boundaries.

Table 2. Data used for object-based image classification.

Rank	Data	Post-Processing	OBIA Application
1	Lidar data TIN* surface		Vector thematic layer
2	Elevation standard deviation	3 × 3 high pass filter & boolean reclassification	Raster data layer
3	Elevation minimum	Boolean reclassification	Raster data layer
4	Total number of points		Raster data layer
5	Total number of points	3 × 3 low pass filter	Raster data layer
6	Total number of points	3 × 3 median filter	Raster data layer
7	Total number of points	3 × 3 Sobel filter	Raster data layer
8	Absolute roughness		Raster data layer
9	Intensity		Raster data layer
10	Point density		Raster data layer
11	Slope		Raster data layer

*TIN: Triangulated Irregular Network

Vector thematic data was created to guide object segmentation and to further refine and isolate downed log object boundaries. A TIN surface was created from the ground lidar points. The triangulated polygons were iteratively masked to isolate polygons based on surface area and resemblance to the linear characteristics of downed logs. Polygons with the largest surface area represent canopy cover while the smallest area polygons represent the ground surface. In between the two extremes are polygons that form the objects of downed logs. Greater polygonal areas are areas with an absence of ground lidar data points and indicate features that are above ground such as logs and crowns in the tree canopy. Further refinement of the TIN surface was achieved through polygonal simplification and aggregation through a polygon point removal algorithm based on polygon area and distance to neighbor thresholds determined through visual interpretation.

4.2. Object-Based Image Analysis

Object-based image analysis was conducted using Trimble's eCognition software formally known as Definiens [83]. eCognition is rule-based OBIA software that supports ancillary vector data and image segmentation and classification. A multiresolution segmentation algorithm was selected to segment the pixel and thematic data layers into objects. After testing multiple segmentation algorithms with an array of specifications and data layer weights the multiresolution segmentation algorithm produced the most optimal object size and shape that most closely encapsulated homogenous and downed log features. The multiresolution segmentation algorithm is a bottom-up method that utilizes a pairwise region merging technique that locally minimizes average object heterogeneity and maximizes homogeneity and consecutively merges pixels and image objects [84]. The reclassified boolean elevation minimum layer and TIN surface thematic layer were used as inputs for segmentation. The elevation minimum layer was assigned a weight of 1 and the following parameters were specified: scale of 1,000, shape of 0.1, and compactness of 0.5. Only one segmentation layer was created after assessing the utility of multiple segmentation layers at a variety of scales.

Three classification categories were used in combination with temporary classes and included: downed logs, canopy cover, and ground. Objects were targeted for classification beginning with the

largest to smallest area objects. Workflow for object classification began with classifying large area ground objects and canopy cover using a combination of object features such as geometry (e.g., area, direction, and rectangular fit) and layer values (e.g., mean, standard deviation, and difference to neighbors). Objects were continuously merged as they were classified. Spurious and smaller objects that were in areas of ground and canopy were merged with the larger classified objects using class related features and algorithms to grow and resize objects based on their position to previously classified canopy and ground objects.

After the larger area objects were classified, the smallest area objects were then classified as ground using class related and layer features such as object area, geometry, and relation to neighboring objects (e.g., borders and distance). The remaining objects to classify consisted of unclassified downed logs and ground objects. Objects resembling downed log features were classified based on their length, width, area, and linearity. The remaining and more dispersed downed logs and ground objects were classified using algorithms and object features related to their position within the scene as opposed to classification based on layer values and object characteristics. Classification based on scene position was required because of the lack of value heterogeneity in objects dispersed throughout the scene. Objects were too similar to each other in terms of object value and characteristics to classify correctly and independent of each other.

4.3. Object-Based Image Analysis Classification Accuracy Assessment

The results of the object-based image analysis classification are assessed for accuracy by comparing areas classified as downed logs to manually digitized interpretations of downed logs. The spatial overlap between the classified log objects and the digitized objects is expressed as percent classified correct. Spatial overlap is defined as the intersection and centroid of the digitized downed log line segments in relation to a classified downed log object.

5. Results

Segmentation and classification was completed using 113 individual object refinement and classification rules with a total processing time of 6 seconds. A total of 13,588 objects were segmented from the input data with areas ranging from 0.25 to 18,842 m^2 with an average area of 8 m^2. As expected, object shapes followed the outlines of features in the thematic TIN surface and resembled unambiguous objects present in the data and landscape (Figure 3). The initial number of objects was reduced to 3,547 through further processing during object refinement and classification.

Table 3 shows statistics for each input data layer for the classified log and ground and canopy objects. Statistics for each input data layer for the log objects are for the most part distinct but are not considerably different from the statistics for the ground and canopy objects. The three data layers that aided the most in classification were the elevation standard deviation, minimum elevation, and the total number of points layers. The total number of points layer filtered by the low-pass, Sobel, and median filters had the most difference between the two class object values, particularly in their minimum and maximum (Table 3). Object geometry statistics show the classified log objects have a mean main direction of 71. This indicates classified logs lay on average in a linear northeast to southwest direction. Classified log object length ranged from 6 to 130 m with a mean of 23 m; the object width

ranged from 4 to 99 m with a mean of 15 m. The mean lengths of classified log objects correspond well to those observed in the field.

Figure 3. Initial objects segmented from input raster and vector thematic data.

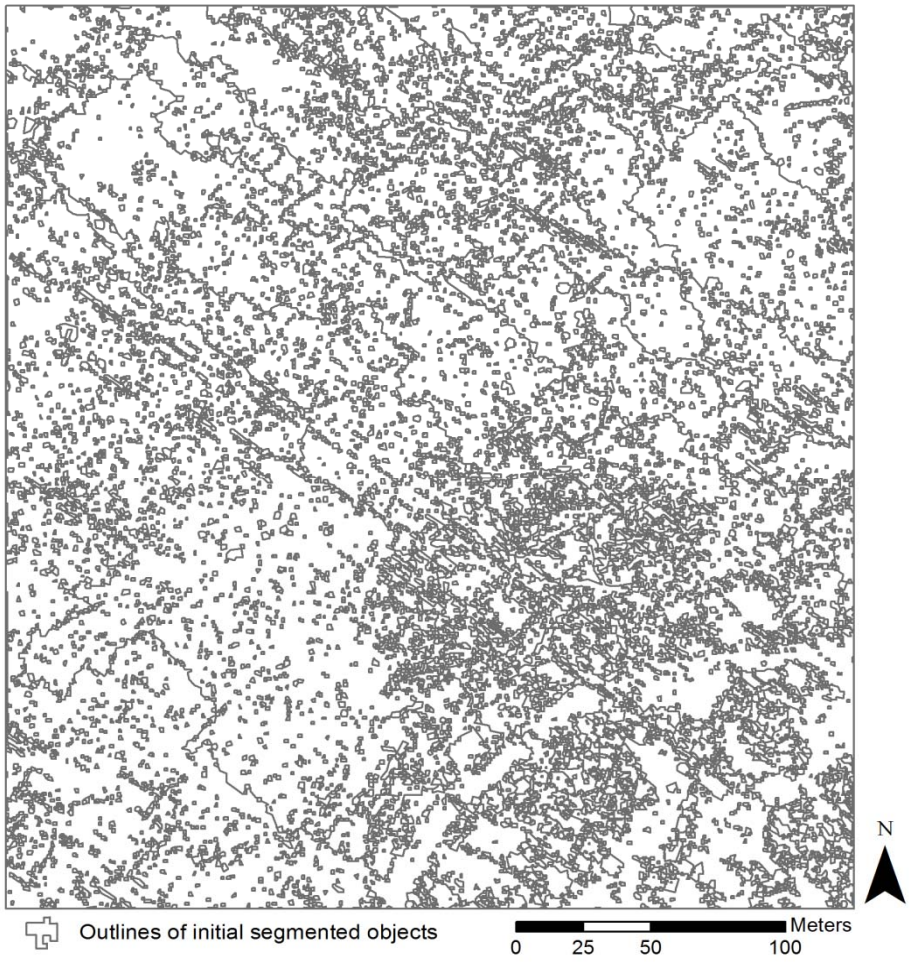

Table 3. Classified object layer statistics*.

		Data Layer									
Class	**Statistic**	Elevation standard deviation[1]	Elevation minimum[2]	Total number of points	Total number of points[3]	Total number of points[4]	Total number of points[5]	Absolute roughness	Intensity	Point density	Slope
Downed logs	Min.	0.34	0.34	0.50	0.44	0.24	3.90	0.05	99.67	13.16	8.63
	Max.	1	0.86	2.61	2.55	2.35	13.69	0.19	153.42	24.32	25.06
	Mean	0.87	0.68	1.40	1.31	1.10	7.86	0.13	118.97	16.65	18.92
Ground & canopy cover	Min.	0	0	0	0	0	0	−1	−1	−1	−1
	Max.	1	1	13	11.51	12.80	68	0.54	968.42	60	55.45
	Mean	0.79	0.68	1.54	1.39	1.16	8.28	0.14	115.79	18.22	20

*Note: [1]3 × 3 high pass filter & boolean reclassification; [2]Boolean reclassification; [3]3 × 3 low pass filter; [4]3 × 3 median filter; [5]3 × 3 Sobel filter.

Figure 4 shows the OBIA classification result in terms of downed logs and the background (ground and canopy cover). Classified downed log object areas ranged from 5 to 686 m^2 with a mean of 55 m^2. These include large merged objects that encompass more than one downed log. A total of 3,470 m^2, or 3 percent of the study area, was classified as downed logs (Figure 4). 76 of the 103 (73%) digitized downed logs were completely or partially classified correctly. Of the 76 logs classified correctly, 60 logs (58 percent overall) have their centroids within a classified log object. Over classification occurred in areas with large numbers of logs clustered in close proximity and in areas with shrub and tree canopy.

Figure 4. Object classification result.

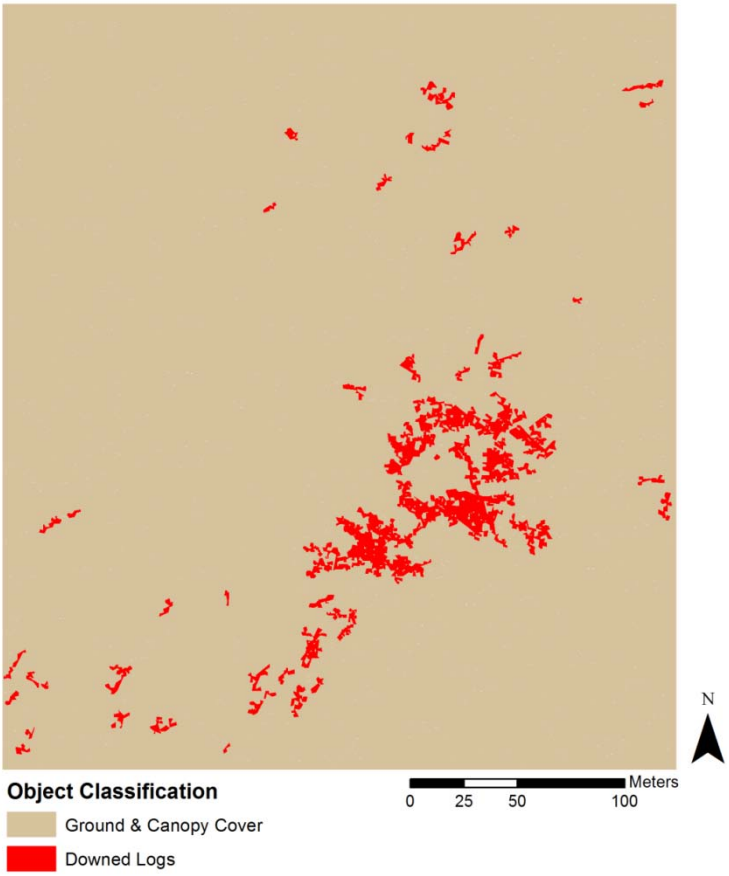

6. Discussion

Downed log objects were successfully delineated and classified from lidar derived metrics using an OBIA framework. The three most useful input data layers in optimizing OBIA object delineation and classification were the TIN surface of lidar points, the elevation minimum, and the total number of points raster layers. These data layers maximized the delineation of discrete linear downed log objects and optimized the classification of log and non-log objects. The result of the classified downed logs yields useful information for characterizing downed logs such as the number and location of downed logs, their distribution and direction on the forest floor, and individual log areas and dimensions.

The majority of classified downed log objects follow a consistent linear pattern and cardinal direction. The dimensions of the correctly classified downed log objects generally agreed well with the dimensions of downed logs in the validation data set and in ground observations. The spatial location,

general outline, and length dimensions of the classified log objects correspond well with the validation data; however, the width of the log objects did not correspond well with the validation data. This is most likely due to non-log objects that are adjacent to correctly classified log objects, are over classified as log objects because their lidar data metric values are similar and difficult to separate.

While the OBIA downed logs classification accuracy was relatively high (73% of the digitized downed logs were classified correctly), misclassification occurred in predictable areas. Over classification of downed logs occurred primarily where clusters of downed logs were found, and where individual and discrete log boundaries were ambiguous in areas of vegetation and tree canopy. Under classification of downed logs occurred mainly for noncontiguous objects that were split into multiple objects by the collection pattern of the lidar sensor inherent in the lidar data point spacing and raster data spatial resolution. Object classification accuracy may be increased through further object boundary refinement, manual editing using positional and relational object features, and image filtering.

Figure 5 provides a detailed example of downed log object misclassification. In Figure 5(a) the linear features of downed logs in a northeast to southwest orientation are visible throughout the scene along with vegetation and canopy cover which are depicted as bright white. In Figure 5(b) the downed log validation layer is overlaid with the input data showing the locations of known downed logs. In Figure 5(c) the final classified object boundaries can be seen encompassing homogenous values in the input data that form around the visible downed logs and ground and canopy pixels. Figure 5(d) shows some of the classification cases: arrow 1 shows over classification, arrow 2 shows under classification, and arrow 3 shows accurate classification.

OBIA classification methods combined with lidar data in this study were not entirely satisfactory in terms of an analyst's time efficiency. While processing time in eCognition only took 6 seconds, the construction of the object segmentation and classification rule set and determination of classification thresholds based on visual interpretation took much longer over multiple days. The majority of classification algorithms were dedicated to classifying the smallest objects. True automation of the OBIA segmentation and classification of downed logs using lidar was not accomplished in this study because of nuances in the data that required visual interpretation and, in some cases, local- and positional-based rule sets that affect specific objects. Classification using fixed thresholds and scene-wide algorithms will allow for a basic classification of downed logs but they are limited. The result would need to be interpreted and edited with spatially explicit thresholds for classification. Object classification based on an object's location within the scene is required. *A priori* and study area specific knowledge of downed log characteristics are also required for determination of the classification thresholds. One of the difficulties in object creation and classification using raw lidar data is dealing with the lidar data point spacing, which creates strips in the rasterized data where homogenous pixels are separated into data value and no data value. This makes homogenous object creation difficult and time consuming.

Figure 5. Detail of object-based image analysis downed log object delineation and classification: **(a)** Total number of points input layer; **(b)** Digitized downed logs reference layer; **(c)** Final object outlines for downed log objects and canopy and ground objects; **(d)** Final classified downed log objects; **(e)** Location of detail in study area.

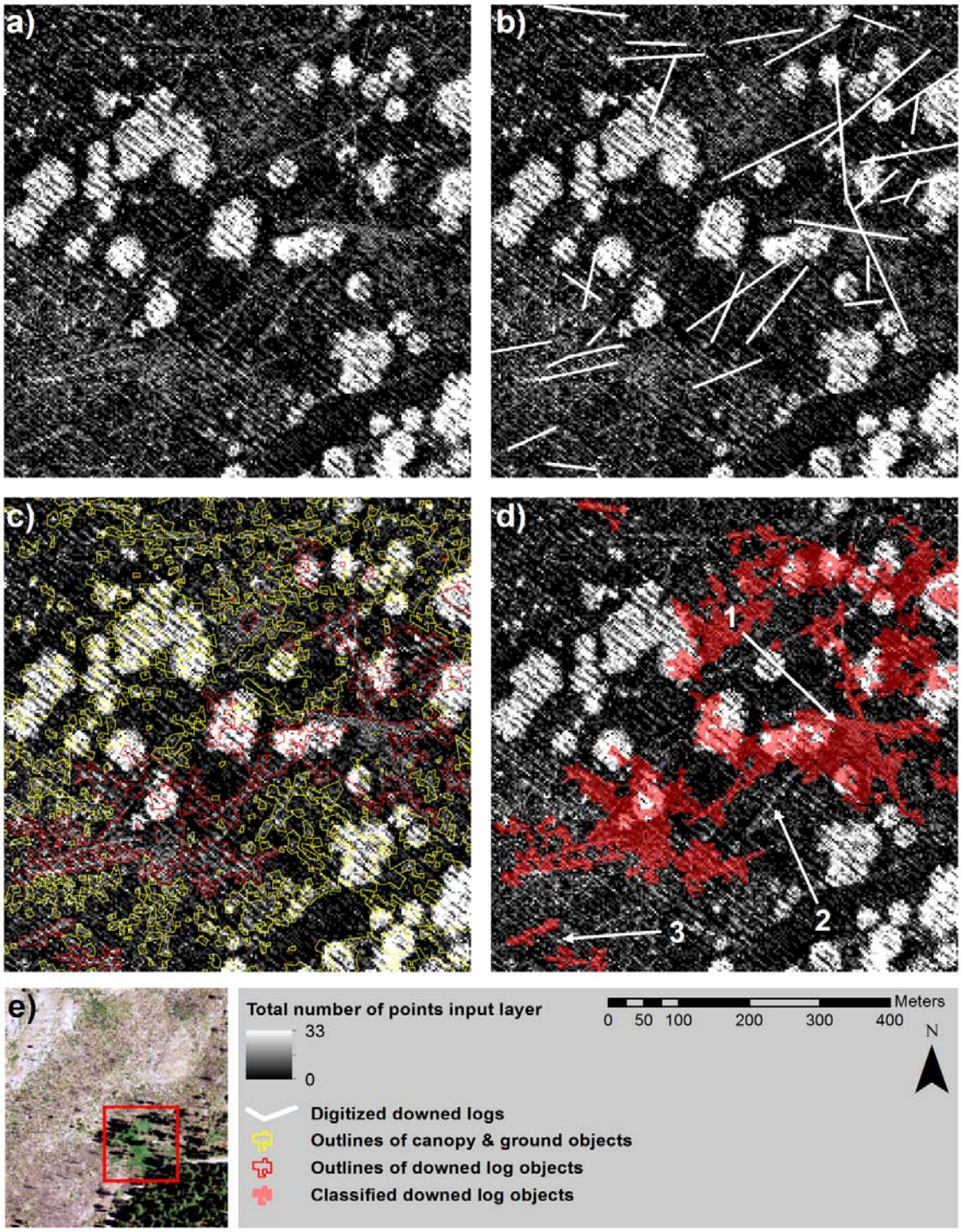

7. Conclusion

The objective of this study was to examine the utility of OBIA methods for identifying and quantifying downed logs in a disturbed, forested landscape using airborne lidar data. Downed log objects and their characteristics were successfully classified and identified using an OBIA approach

with relatively high classification accuracies. While downed log objects were successfully extracted, the lidar data and OBIA methods proved to be inefficient due to the amount of time required and difficulty in delineating whole and homogenous downed log objects in the lidar data.

The main conclusions drawn from this study are: (1) Downed log objects were successfully delineated using lidar derived metrics using an OBIA framework. (2) The downed log object classification accuracy was relatively high (73% of the digitized downed logs were classified correctly). (3) The classified downed log objects yield useful information that can be used to help characterize logs on the forest floor. (4) Lidar data coupled with an OBIA framework for classifying downed logs on the forest floor was effective but inefficient in terms of: (a) substantial analyst time was required for manual and positional-based rule sets and visual interpretation; (b) OBIA rule set automation was not achieved; (c) the methodological inefficiency is related most to the data structure of the lidar data than the OBIA framework where homogenous objects in the lidar data are difficult to extract. (5) Airborne lidar data coupled with OBIA techniques can be used to compliment but not replace field based methods for identifying and characterizing understory downed logs in forests.

OBIA and lidar have been used independently and to great impact in forest science research; this paper demonstrates a novel combination of these new remote sensing technologies. Mapping downed logs on the forest floor is a particularly challenging problem: airborne lidar is very effective at mapping fine scale topography in forests [30], and at mapping above ground forest structure [24], but downed logs on the forest floor are a considerable challenge to map completely. The raw lidar data processed into raster layers such as number of points per area, elevation, and standard deviation of elevation did reveal the downed logs, but their classification still required considerable analyst interpretation. Thus the OBIA methods were effective but inefficient in the delineation and classification of downed logs based on lidar data. Consequently, field data collection will continue to be important for mapping these features; but possibly ground-based lidar data will provide new avenues for mapping ground features. Recently, new types of ground-based lidar sensors have shown promise for extracting forest stand structural parameters, such as diameter at breast height (DBH), stem count density, basal area, and above-ground woody biomass with high accuracy [85]. When coupled with new processing methods that include OBIA, these data will undoubtedly play an increased role in the detailed mapping of forests, and in particular in the mapping of forest understory.

Acknowledgments

This paper is SNAMP Publication Number #7. The Sierra Nevada Adaptive Management Project is funded by USDA Forest Service Region 5, USDA Forest Service Pacific Southwest Research Station, US Fish and Wildlife Service, California Department of Water Resources, California Department of Fish and Game, California Department of Forestry and Fire Protection, and the Sierra Nevada Conservancy. Ecognition software was made available through the Berkeley Geospatial Innovation Facility.

References

1. Kueppers, L.M.; Southon, J.; Baer, P.; Harte, J. Dead wood biomass and turnover time, measured by radiocarbon, along a subalpine elevation gradient. *Oecologia* **2004**, *141*, 641-651.

2. Schiegg, K. Effects of dead wood volume and connectivity on saproxylic insect species diversity. *Ecoscience* **2000**, *7*, 290-298.
3. Dixon, R.K.; Solomon, A.; Brown, S.; Houghton, R.; Trexier, M.; Wisniewski, J. Carbon pools and flux of global forest ecosystems. *Science* **1994**, *263*, 185.
4. Scott, J.H.; Burgan, R.E. *Standard Fire Behavior Fuel Models: A Comprehensive Set for Use with Rothermel's Surface Fire Spread Model*; USDA Forest Service, Rocky Mountain Research Station: Fort Collins, CO, USA, 2005; p. 72.
5. van Wagtendonk, J.W.; Benedict, J.M.; Sydoriak, W.M. Fuel bed characteristics of Sierra Nevada conifers. *Western J. Appl. Forest.* **1998**, *13*, 73-84.
6. Janisch, J.; Harmon, M. Successional changes in live and dead wood carbon stores: Implications for net ecosystem productivity. *Tree Physiol.* **2002**, *22*, 77.
7. Pesonen, A.; Maltamo, M.; Eerikainen, K.; Packalen, P. Airborne laser scanning-based prediction of coarse woody debris volumes in a conservation area. *Forest Ecol. Manage.* **2008**, *255*, 3288-3296.
8. Rouvinen, S.; Kuuluvainen, T. Amount and spatial distribution of standing and downed dead trees in two areas of different fire history in a boreal Scots pine forest. *Ecol. Bull.* **2001**, *49*, 115-127.
9. Bobiec, A. Living stands and dead wood in the Biaowiea forest: Suggestions for restoration management. *Forest Ecol. Manage.* **2002**, *165*, 125-140.
10. Christensen, M.; Hahn, K.; Mountford, E.P.; Odor, P.; Standovar, T.; Rozenbergar, D.; Diaci, J.; Wijdeven, S.; Meyer, P.; Winter, S. Dead wood in European beech (*Fagus sylvatica*) forest reserves. *Forest Ecol. Manage.* **2005**, *210*, 267-282.
11. Butler, R.; Angelstam, P.; Ekelund, P.; Schlaepfer, R. Dead wood threshold values for the three-toed woodpecker presence in boreal and sub-Alpine forest. *Biol. Conserv.* **2004**, *119*, 305-318.
12. Jordan, G.J.; Ducey, M.J.; Gove, J.H. Comparing line-intersect, fixed-area, and point relascope sampling for dead and downed coarse woody material in a managed northern hardwood forest. *Can. J. Forest Res.* **2004**, *34*, 1766-1775.
13. Pasher, J.; King, D.J. Mapping dead wood distribution in a temperate hardwood forest using high resolution airborne imagery. *Forest Ecol. Manage.* **2009**, *258*, 1536-1548.
14. Wilson, E.H.; Sader, S.A. Detection of forest harvest type using multiple dates of Landsat TM imagery. *Remote Sens. Environ.* **2002**, *80*, 385-396.
15. Sader, S.A. Spatial characteristics of forest clearing and vegetation regrowth as detected by Landsat Thematic Mapper imagery. *Photogramm. Eng. Remote Sensing* **1995**, *61*, 1145-1151.
16. Asner, G.P.; Palace, M.; Keller, M.; Pereira Jr, R.; Silva, J.N.M.; Zweede, J.C. Estimating canopy structure in an Amazon forest from Laser Range Finder and IKONOS satellite observations. *Biotropica* **2002**, *34*, 483-492.
17. Kayitakire, F.; Hamel, C.; Defourny, P. Retrieving forest structure variables based on image texture analysis and IKONOS-2 imagery. *Remote Sens. Environ.* **2006**, *102*, 390-401.
18. Wulder, M.A.; Dymond, C.C.; White, J.C.; Leckie, D.G.; Carroll, A.L. Surveying mountain pine beetle damage of forests: A review of remote sensing opportunities. *Forest Ecol. Manage.* **2006**, *221*, 27-41.
19. De Chant, T.; Kelly, M. Individual object change detection for monitoring the impact of a forest pathogen on a hardwood forest. *Photogramm. Eng. Remote Sensing* **2009**, *75*, 1005-1014.

20. Clark, D.B.; Castro, C.S.; Alvarado, L.D.A.; Read, J.M. Quantifying mortality of tropical rain forest trees using high spatial resolution satellite data. *Ecol. Lett.* **2004**, *7*, 52-59.
21. Guo, Q.C.; Kelly, M.; Gong, P.; Liu, D. An object-based classification approach in mapping tree mortality using high spatial resolution imagery. *GISci. Remote Sens.* **2007**, *44*, 24-47.
22. Lefsky, M.A.; Cohen, W.B.; Spies, T.A. An evaluation of alternate remote sensing products for forest inventory, monitoring, and mapping of Douglas-fir forests in western Oregon. *Can. J. Forest Res.* **2001**, *31*, 78-87.
23. Lefsky, M.A.; Cohen, W.B.; Parker, G.G.; Harding, D.J. Lidar remote sensing for ecosystem studies. *BioScience* **2002**, *52*, 19-30.
24. Vierling, K.T.; Vierling, L.A.; Gould, W.A.; Martinuzzi, S.; Clawges, R.M. Lidar: Shedding new light on habitat characterization and modeling. *Front. Ecol. Environ.* **2008**, *6*, 90-98.
25. Seavy, N.E.; Viers, J.H.; Wood, J.K. Riparian bird response to vegetation structure: A multiscale analysis using LiDAR measurements of canopy height. *Ecol. Appl.* **2009**, *19*, 1848-1857.
26. Dubayah, R.; Drake, J. Lidar remote sensing for forestry. *J. Forest.* **2000**, *98*, 44-46.
27. Lefsky, M.A.; Cohen, W.B.; Harding, D.J.; Parker, G.G.; Acker, S.A.; Gower, S.T. Lidar remote sending of above-ground biomass in three biomes. *Global Ecol. Biogeogr.***2002**, *11*, 393-399.
28. Reutebuch, S.; Andersen, H.; McGaughey, R. Light detection and ranging (LIDAR): An emerging tool for multiple resource inventory. *J. Forest.* **2005**, *103*, 286-292.
29. Hummel, S.; Hudak, A.; Uebler, E.; Falkowski, M.; Megown, K. A comparison of accuracy and cost of LiDAR *versus* stand exam data for landscape management on the Malheur National Forest. *J. Forest.* **2011**, *109*, 267-273.
30. Guo, Q.; Li, W.; Yu, H.; Alvarez, O. Effects of topographic variability and lidar sampling density on several DEM interpolation methods. *Photogramm. Eng. Remote Sensing* **2010**, *76*, 701-712.
31. Antonarakis, A.S.; Richards, K.S.; Brasington, J. Object-based land cover classification using airborne LiDAR. *Remote Sens. Environ.* **2008**, *112*, 2988-2998.
32. Hyyppä, J.; Kelle, O.; Lehikoinen, M.; Inkinen, M. A segmentation-based method to retrieve stem volume estimates from 3-D tree height models produced by laser scanners. *IEEE Trans. Geosci. Remote Sens.* **2001**, *39*, 969-975.
33. Popescu, S.C.; Wynne, R.H.; Nelson, R.F. Measuring individual tree crown diameter with lidar and assessing its influence on estimating forest volume and biomass. *Can. J. Remote Sens.* **2003**, *29*, 564-577.
34. Naesset, E.; Gobakken, T. Estimation of above- and blow-ground biomass across regions of the boreal forest zone using airborne laser. *Remote Sens. Environ.* **2008**, *112*, 3079-3090.
35. Morsdorf, F.; Kötz, B.; Meier, E.; Itten, K.I.; Allgöwer, B. Estimation of LAI and fractional cover from small footprint airborne laser scanning data based on gap fraction. *Remote Sens. Environ.* **2006**, *104*, 50-61.
36. Brandtberg, T.; Warner, T.A.; Landenberger, R.E.; McGraw, J.B. Detection and analysis of individual leaf-off tree crowns in small footprint, high sampling density lidar data from the eastern deciduous forest in North America. *Remote Sens. Environ.* **2003**, *85*, 290-303.
37. Chen, Q.; Baldocchi, D.; Gong, P.; Kelly, M. Isolating individual trees in a savanna woodland using small footprint LIDAR data. *Photogramm. Eng. Remote Sensing* **2006**, *72*, 923-932.

38. Koch, B.; Heyder, U.; Weinacker, H. Detection of individual tree crowns in airborne lidar data. *Photogramm. Eng. Remote Sensing* **2006**, *72*, 357-363.
39. Popescu, S.C.; Wynne, R.H. Seeing the trees in the forest: Using lidar and multispectral data fusion with local filtering and variable window size for estimating tree height. *Photogramm. Eng. Remote Sensing* **2004**, *70*, 589-604.
40. Suarez, J.C.; Ontiveros, C.; Smith, S.; Snape, S. Use of airborne LiDAR andaerial photography in the estimation of individual tree heights in forestry. *Comput. Geosci.* **2005**, *31*, 253-262.
41. Wing, M.G.; Eklund, A.; Sessions, J. Applying LiDAR technology for tree measurements in burned landscapes. *Int. J. Wildland Fire* **2010**, *19*, 104-114.
42. Kim, Y.; Yang, Z.; Cohen, W.B.; Pflugmacher, D.; Lauver, C.L.; Vankat, J.L. Distinguishing between live and dead standing tree biomass on the North Rim of Grand Canyon National Park, USA using small-footprint lidar data. *Remote Sens. Environ.* **2009**, *113*, 2499-2510.
43. Seielstad, C.A.; Queen, L.P. Using airborne laser altimetry to determine fuel models for estimating fire behavior. *J. Forest.* **2003**, *101*, 10-15.
44. Andersen, H.-E.; McGaughey, R.J.; Reutebuch, S.E. Estimating forest canopy fuel parameters using LIDAR data. *Remote Sens. Environ.* **2005**, *94*, 441-449.
45. Erdody, T.L.; Moskal, L.M. Fusion of LiDAR and imagery for estimating forest canopy fuels *Remote Sens. Environ.* **2010**, *114*, 725-737.
46. Riaño, D.; Meier, E.; Allgöwer, B.; Chuvieco, E.; Ustin, S.L. Modeling airborne laser scanning data for the spatial generation of critical forest parameters in fire behavior modeling. *Remote Sens. Environ.* **2003**, *86*, 177-186.
47. Garcia-Feced, C.; Temple, D.J.; Kelly, M. Characterizing California Spotted Owl nest sites and their associated forest stands using Lidar data. *J. Forest.* **2011**, in press.
48. Hinsley, S.; Hill, R.; Bellamy, P.; Balzter, H. The application of lidar in woodland bird ecology: Climate, canopy structure, and habitat quality. *Photogramm. Eng. Remote Sensing* **2006**, *72*, 1399.
49. Nelson, R.; Keller, C.; Ratnaswamy, M. Locating and estimating the extent of Delmarva fox squirrel habitat using an airborne LiDAR profiler. *Remote Sens. Environ.* **2005**, *96*, 292-301.
50. Hyde, P.; Dubayah, R.; Walker, W.; Blair, J.B.; Hofton, M.; Hunsaker, C. Mapping forest structure for wildlife habitat analysis using multi-sensor (LiDAR, SAR/InSAR, ETM+, Quickbird) synergy. *Remote Sens. Environ.* **2006**, *102*, 63-73.
51. Goetz, S.; Steinberg, D.; Dubayah, R.; Blair, B. Laser remote sensing of canopy habitat heterogeneity as a predictor of bird species richness in an eastern temperate forest, USA. *Remote Sens. Environ.* **2007**, *108*, 254-263.
52. Müller, J.; Stadler, J.; Brandl, R. Composition *versus* physiognomy of vegetation as predictors of bird assemblages: The role of lidar. *Rem Sens. Environ.* **2010**, *114*, 490-495.
53. Martinuzzi, S.; Vierling, L.A.; Gould, W.A.; Falkowski, M.J.; Evans, J.S.; Hudak, A.T.; Vierling, K.T. Mapping snags and understory shrubs for a LiDAR-based assessment of wildlife habitat suitability. *Remote Sens. Environ.* **2009**, *113*, 2533-2546.
54. Bunting, P.; Lucas, R.M.; Jones, K.; Bean, A.R. Characterisation and mapping of forest communities by clustering individual tree crowns. *Remote Sens. Environ.* **2010**, *114*, 2536-2547.
55. Omasa, K.; Qiu, G.Y.; Watanuki, K.; Yoshimi, K.; Akiyama, Y. Accurate estimation of forest carbon stocks by 3-D remote sensing of individual trees. *Environ. Sci. Technol.* **2003**, *37*, 1198-1201.

56. Liu, D.; Kelly, M.; Gong, P. A spatial-temporal approach to monitoring forest disease spread using multi-temporal high spatial resolution imagery. *Remote Sens. Environ.* **2006**, *101*, 167-180.
57. Kelly, M.; Meentemeyer, R.K. Landscape dynamics of the spread of sudden oak death. *Photogramm. Eng. Remote Sensing* **2002**, *68*, 1001-1009.
58. Benz, U.C.; Hofmann, P.; Willhauck, G.; Lingenfelder, I.; Heynen, M. Multi-resolution, object-oriented fuzzy analysis of remote sensing data for GIS-ready information. *ISPRS J. Photogramm.* **2004**, *58*, 239-258.
59. Blaschke, T. Object based image analysis for remote sensing. *ISPRS J. Photogramm.* **2010**, *65*, 2-16.
60. Chubey, M.S.; Franklin, S.E.; Wulder, M.A. Object-based analysis of Ikonos-2 imagery for extraction of forest inventory parameters. *Photogramm. Eng. Remote Sensing* **2006**, *72*, 383-394.
61. Flanders, D.; Hall-Beyer, M.; Pereverzoff, J. Preliminary evaluation of eCognition object-based software for cut block delineation and feature extraction. *Can. J. Remote Sens.* **2003**, *29*, 441-452.
62. Su, W.; Zhang, C.; Yang, J.; Wu, H.; Chen, M.; Yue, A.; Zhang, Y.; Sun, C. Knowledge-based object oriented land cover classification using SPOT5 imagery in forest-agriculture ecotones. *Sens. Lett.* **2010**, *8*, 22-31.
63. Cleve, C.; Kelly, M.; Kearns, F.; Moritz, M. Classification of urban environments for fire management support: A comparison of pixel- and object-based classifications using high-resolution aerial photography. *Comput. Environ. Urban Syst.* **2008**, *32*, 317-326.
64. Liu, Y.; Guo, Q.; Kelly, M. A framework of region-based spatial relationships for non-overlapping features and its application in object based image analysis. *ISPRS J. Photogramm.* **2008**, *63*, 461-475.
65. Burnett, C.; Blaschke, T. A multi-scale segmentation/object relationship modeling methodology for landscape analysis. *Ecol. Model.* **2003**, *168*, 233-249.
66. Hay, G.J.; Castilla, G. Object-Based Image Analysis: Strengths, Weaknesses, Opportunities and Threats (SWOT). In *Proceedings of 1st International Conference on Object-Based Image Analysis (OBIA 2006)*, Salzburg, Austria, 4–5 July 2006; In *IAPRS*; 2006; Volume XXXVI.
67. Van Coillie, F.M.B.; Verbeke, L.P.C.; Wulf, R.R.D. Feature selection by genetic algorithms in object-based classification of IKONOS imagery for forest mapping in Flanders, Belgium. *Remote Sens. Environ.* **2007**, *110*, 476-487.
68. Hay, G.J.; Castilla, G.; Wulder, M.A.; Ruiz, J.R. An automated object-based approach for the multiscale image segmentation of forest scenes. *Int. J. Appl. Earth Obs. Geoinf.* **2005**, *7*, 339-359.
69. Kim, M.; Madden, M.; Warner, T.A. Forest type mapping using object-specific texture measures from multispectral Ikonos imagery: Segmentation quality and image classification issues. *Photogramm. Eng. Remote Sensing* **2009**, *75*, 819-830.
70. Sullivan, A.A.; McGaughey, R.J.; Andersen, H.E.; Schiess, P. Object-oriented classification of forest structure from light detection and ranging data for stand mapping. *Western J. Appl. Forest.* **2009**, *24*, 198-204.
71. Yu, Q.; Gong, P.; Clinton, N.; Kelly, M.; Schirokauer, D. Object-based detailed vegetation classification with airborne high spatial resolution remote sensing imagery. *Photogramm. Eng. Remote Sensing* **2006**, *72*, 799-811.
72. De Chant, T.; Gallego, A.H.; Saornil, J.V.; Kelly, M. Urban influence on changes in linear forest edge structure. *Landscape Urban Plan.* **2010**, *96*, 12-18.

73. Arroyo, L.A.; Johansen, K.; Armston, J.; Phinn, S. Integration of LiDAR and QuickBird imagery for mapping riparian biophysical parameters and land cover types in Australian tropical savannas. *Forest Ecol. Manage.* **2010**, *259*, 598-606.
74. Johansen, K.; Arroyo, L.; Armston, J.; Phinn, S.; Witte, C. Mapping riparian condition indicators in a sub-tropical savanna environment from discrete return LiDAR data using object-based image analysis. *Ecol. Indic.* **2010**, *10*, 796-807.
75. Pascual, C.; García-Abril, A.; García-Montero, L.G.; Martín-Fernandez, S.; Cohen, W.B. Object-based semi-automatic approach for forest structure characterization using lidar data in heterogeneous Pinus sylvestris stands. *Plant Ecol. Manage.* **2008**, *255*, 3677-3685.
76. Johansen, K.; Tiede, D.; Blaschke, T.; Arroyo, L.A.; Phinn, S. Automatic geographic object based mapping of streambed and riparian zone extent from LiDAR data in a temperate rural urban environment, Australia. *Remote Sens.* **2011**, *3*, 1139-1156.
77. Arroyo, L.A.; Healey, S.P.; Cohen, W.B.; Cocero, D.; Manzanera, J.A. Using object-oriented classification and high-resolution imagery to map fuel types in a Mediterranean region. *J. Geophys. Res.* **2006**, doi:10.1029/2005JG000120.
78. Kim, M.; Madden, M.; Xu, B. GEOBIA vegetation mapping in Great Smoky Mountains National Park with spectral and non-spectral ancillary information. *Photogramm. Eng. Remote Sensing* **2010**, *76*, 137-149.
79. SNAMP Sierra Nevada Adaptive Management Program (SNAMP). Available online: http://snamp.cnr.berkeley.edu/ (accessed on 8 March 2011).
80. NCALM National Center for Airborne Laser Mapping (NCALM). Available online: http://www.ncalm.cive.uh.edu/ (accessed on 8 March 2011).
81. Terrasolid TerraScan. Available online: http://www.terrasolid.fi/en (accessed on 8 March 2011).
82. USDA National Agriculture Imagery Program (NAIP). Available online: http://www.fsa.usda.gov/FSA/apfoapp?area=home&subject=prog&topic=nai (accessed on 8 March 2011).
83. Trimble eCognition. Available online: http://www.ecognition.com/ (accessed on 8 March 2011).
84. Trimble. *eCognition Developer 8.64.0: User Guide*; 8.64.0 ed.; Trimble: Munich, Germany, 2010.
85. Yao, T.; Yang, X.; Zhao, F.; Wang, Z.; Zhang, Q.; Jupp, D.; Lovell, J.; Culvenor, D.; Newnham, G.; Ni-Meister, W. Measuring forest structure and biomass in New England forest stands using Echidna ground-based lidar. *Remote Sens. Environ.* **2011**, doi:10.1016/j.rse.2010.03.019.